IEEE Access
Multidisciplinary ⋮ Rapid Review ⋮ Open Access Journal

Received July 14, 2020, accepted July 25, 2020, date of publication July 28, 2020, date of current version August 7, 2020.

Digital Object Identifier 10.1109/ACCESS.2020.3012611

STAP for Airborne Radar Based on Dual-Frequency Space-Time Coprime Sampling Structure

MINGXIN LIU[1], BIN TANG[1,2], (Member, IEEE), XIAOXIA ZHENG[1,2], QIANG WANG[1], SIYUAN WANG[1], XU WANG[1], MENGXU FANG[1], JING ZHU[1], AND CHENGLONG FENG[1]

[1]School of General Aviation, Chengdu Aeronautic Polytechnic, Chengdu 610100, China
[2]College-Enterprise Joint Avionics Innovation Base in Sichuan, Chengdu 610100, China

Corresponding author: Mingxin Liu (lmx0951@163.com)

This work was supported in part by the Key Project of Sichuan Provincial Department of Education under Grant 18ZA0034, in part by the Project of Sichuan Provincial Department of Education under Grant 16ZB0389, and in part by the Project of Sichuan Provincial Department of Education under Grant 17ZB0038.

ABSTRACT To overcome the space-time adaptive processing (STAP) performance loss caused by discarding the non-uniform parts of difference coarray and copulse for coprime sampling structure under the condition of single-frequency operation, this paper proposes a new STAP algorithm to improve the precision of filter weight vector estimation by the dual-frequency operation. By selecting a single proper additional operation frequency, we can obtain the different coarray and copulse, thus fill two missed virtual sensors and pulses of the difference structures in the single-frequency operation simultaneously. Compared with the single-frequency operation, the dual-frequency operation method can acquire the bigger uniform linear array (ULA) and coherent processing interval (CPI) pulse train to improve the system degrees of freedom (DOF), and result in higher angle-Doppler resolution. In addition, the coprime array has the little mutual coupling effect because of the larger inter-sensors spacing. Therefore, the resulting method can alleviate mutual coupling and enhance the system DOF.

INDEX TERMS Coprime sampling structure, degrees of freedom, dual-frequency operation, space-time adaptive processing, mutual coupling.

I. INTRODUCTION

Space-time adaptive processing (STAP) which can improve the ability of suppressing clutter and detecting targets plays a fundamental role in airborne radar [1]–[3]. The traditional algorithms, such as reduced-rank [4]–[8], reduced-dimension [9]–[11] and parameterized model [12]–[25] STAP usually have high detection precision based on the accurate space-time steering vector. However, their performance degrades significantly and even cannot work in the presence of mutual coupling. In actual radar systems, it is necessary to consider the mutual coupling effect. Therefore, the STAP considering mutual coupling is one of the hot issues in radar signal processing.

Generally, researchers mainly focused on the uniform linear array (ULA), in which the inter-sensors spacing was $\lambda/2$ to avoid spatial aliasing. In a previous study, the mutual coupling calibration and compensation were usually realized by hardware, such as adding calibration sensors and adopting low coupling components. However, these methods are not easy to implement in many applications, with the relatively high cost and low accuracy. In the following research, the calibration and compensation of mutual coupling were gradually transformed into an array parameters estimation [26], [27]. In the past, domestic and overseas scholars had proposed many direction of arrival estimation methods under mutual coupling [26]–[30]. However, many algorithms need a multi-dimensional search and multi-parameter optimization [26], [27], which cannot guarantee the global convergence. It is generally known that the induction current between inter-sensors produces electromagnetic coupling in ULA, which changes the magnetic fields near the sensors and affects the space steering vector. The smaller the inter-sensors spacing, the stronger the mutual coupling effect. The inter-sensors spacing of coprime array is larger than $\lambda/2$, and its mutual coupling effect is less severe than that

The associate editor coordinating the review of this manuscript and approving it for publication was Yingsong Li.

of ULA. At the same time, the array aperture can be effectively expanded to improve the degrees of freedom (DOF) by difference operation. Because of this, the coprime array has become a research hot spot in the field of array signal processing in recent years.

The coprime array is a special kind of non-uniform sparse array. Compared with the minimum redundancy array, the array layout of the coprime array is simpler. Compared with the nested array, the coprime array has the less mutual coupling effect. However, the coarray of coprime array has holes, which means that the ULA part of the coarray is smaller than those of the nested array. According to the array layout, the difference coarray can be divided into three difference subarrays by two symmetrical holes. One is the uniform subarray in the middle, the other two are the non-uniform subarrays at the ends of difference coarray, in which the uniform subarray is the main part of the difference coarray. However, two non-uniform subarrays are discarded to cause DOF loss in its application due to the holes. That is to say, the DOF provided by the coprime array is not fully utilized [31]–[34].

Considering the holes distribution in the coarray of the coprime array. This paper uses an additional operation frequency w_h to expand the ULA part of the coarray by filling two symmetrical holes between the uniform subarray and the two non-uniform subarrays at the working frequency w_0, thus the $2N_1$ sensors including the filled holes are absorbed into the uniform subarray. Therefore, a virtual ULA with $2N_1N_2 + 4N_1 - 1$ sensors can be formed by using the dual-frequency operation. For the pulse train, we can obtain a virtual CPI pulse train possessed $2M_1M_2 + 4M_1 - 1$ pulse to improve the temporal domain DOF in the same way. The total DOF of our proposed algorithm increases by $D_I = 4N_1N_2M_1 + 4N_1M_1M_2 + 12N_1M_1 - 2N_1 - 2M_1$ compared to the single-frequency operation. In addition, to avoid the complex spatial-temporal smoothing, this paper uses the matrix increment-rank method to construct the virtual clutter covariance matrix (CCM) for STAP filter weight vector estimation. The numerical simulation results verify the effectiveness of the proposed algorithm.

We outline this paper as follows. In Section II, we provide some fundamental preliminaries of signal model and review the mutual coupling, and present the motivation of this paper. We derive the dual-frequency coprime sampling structure to construct the proposed STAP in Section III. Section IV gives the comparisons between the proposed STAP and other methods versus DOF and mutual coupling effect. Section V concludes this paper.

Notations: lowercase, bold lowercase and bold capital letters represent scalars, vectors and matrices, respectively. Transpose and complex conjugate transpose are denoted by $(\cdot)^T$ and $(\cdot)^H$ respectively. The symbols $\otimes$, $E(\cdot)$, and $|\cdot|$ stand for the Kronecker product, the statistical expectation and the absolute respectively. $\mathbf{I}_M$ stands for the $M \times M$ identity matrix, and $diag(\mathbf{a})$ represents a diagonal matrix whose diagonal elements are the column vector $\mathbf{a}$.

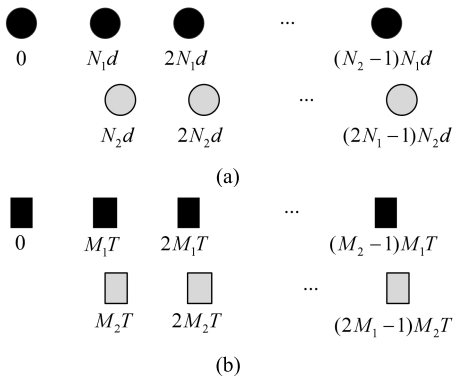

FIGURE 1. Coprime configuration (a) coprime array (b) coprime PRI.

II. PRELIMINARIES

To begin with, we will introduce some fundamental preparations about STAP with coprime sampling structure.

A. SIGNAL MODEL

Assumed that a side-looking airborne phased array radar has N receiving sensors and M transmitting pulses in a coherent processing interval (CPI). The velocity of the radar is v, and the radar wavelength is λ. The receiving array is composed of two sub-ULAs. One possesses N_2 sensors with locations $\{N_1p_2d, 0 \le p_2 \le N_2 - 1\}$, the other has $2N_1 - 1$ sensors at position $\{N_2p_1d, 1 \le p_1 \le 2N_1 - 1\}$, N_1 and N_2 are coprime integers with $N_1 < N_2$, d is the minimal inter-sensors spacing, as shown in Fig. 1(a). As seen in Fig. 1(b), the pulses locations of two sub-pulses are $\{M_1q_2T, 0 \le q_2 \le M_2 - 1\}$ and $\{M_2q_1T, 1 \le q_1 \le 2M_1 - 1\}$ respectively, where M_1 and M_2 are coprime integers with $M_1 < M_2$, T means the minimal pulse repetition interval (PRI). When the working frequency is w, the received clutter plus noise data from a range bin without the ranger ambiguity can be given by

$$\mathbf{x}_u(w) = \sum_{i=1}^{N_c} a_{c,i}\mathbf{v}(\varphi_{c,i}(w), f_{c,i}(w)) + \mathbf{n}(w), \tag{1}$$

where $\mathbf{n}(w)$ is the Gaussian white noise vector whose power is σ_n^2. N_c is the number of independent clutter patches in azimuth domain, $a_{c,i}$ represents the *ith* clutter patch complex gain. The corresponding space-time steering vector $\mathbf{v}(\varphi_{c,i}(w), f_{c,i}(w))$ can be expressed by

$$\mathbf{v}(\varphi_{c,i}(w), f_{c,i}(w)) = \mathbf{v}(\varphi_{c,i}(w)) \otimes \mathbf{v}(f_{c,i}(w)) \tag{2}$$

with

$$\mathbf{v}(\varphi_{c,i}(w)) = [1, e^{2\pi j n_1 \varphi_{c,i}(w)}, \ldots, e^{2\pi j n_{N-1} \varphi_{c,i}(w)}]^T, \tag{3}$$
$$\mathbf{v}(f_{c,i}(w)) = [1, e^{2\pi j m_1 f_{c,i}(w)}, \ldots, e^{2\pi j m_{M-1} f_{c,i}(w)}]^T, \tag{4}$$

where

$$n_\alpha \in \{N_1p_2 \cup N_2p_1\}, \quad \alpha = 1, \cdots, N-1, \tag{5}$$
$$m_\beta \in \{M_1q_2 \cup M_2q_1\}, \quad \beta = 1, \cdots, M-1, \tag{6}$$
$$\varphi_{c,i}(w) = d\cos(\theta_i)/\lambda, \tag{7}$$
$$f_{c,i}(w) = (2vT\cos(\theta_i))/\lambda \tag{8}$$

in which $\varphi_{c,i}(w)$ and $f_{c,i}(w)$ are the normalized spatial and temporal frequency of the *ith* clutter patch, respectively, and θ_i is the space cone angle of *i*th clutter patch. By substituting (7) and (8) into (3) and (4), we can get

$$\mathbf{v}(\varphi_{c,i}(w)) = [1, e^{2\pi j n_1 d\cos(\theta_i)/\lambda}, \ldots, e^{2\pi j n_{N-1} d\cos(\theta_i)/\lambda}]^T, \tag{9}$$

$$\mathbf{v}(f_{c,i}(w)) = [1, e^{2\pi j m_1 T 2v\cos(\theta_i)/\lambda}, \ldots, e^{2\pi j m_{M-1} T 2v\cos(\theta_i)/\lambda}]^T, \tag{10}$$

and further we have

$$\mathbf{v}(\varphi_{c,i}(w)) = [1, e^{jkn_1 d\cos(\theta_i)}, \ldots, e^{jkn_{N-1} d\cos(\theta_i)}]^T, \tag{11}$$

$$\mathbf{v}(f_{c,i}(w)) = [1, e^{jkm_1 T 2v\cos(\theta_i)}, \ldots, e^{jkm_{M-1} T 2v\cos(\theta_i)}]^T, \tag{12}$$

where $k = w/c$ is the wave number in w, c is the velocity of light. Therefore, $\mathbf{v}(\varphi_{c,i}(w), f_{c,i}(w))$ can be described as

$$\mathbf{v}(\varphi_{c,i}(w), f_{c,i}(w)) = \left[s_{0,i}(w), s_{1,i}(w), \cdots, s_{NM-1,i}(w)\right]^T, \tag{13}$$

where

$$\begin{aligned} s_{lM+r-1,i}(w) &= \exp(2\pi j(n_l\varphi_{c,i} + m_{r-1}f_{c,i})) \\ &= \exp(j(kn_l d\cos(\theta_i) + km_{r-1}T2v\cos(\theta_i))) \end{aligned} \tag{14}$$

with $l = 0, \cdots, N-1$, $r = 1, \cdots, M$, $i = 1, \cdots, N_c$. Assuming that the different clutter patches are independent, the clutter plus noise covariance matrix (CNCM) can be formulated as

$$\mathbf{R}_u(w) = E\left[\mathbf{x}_u(w)\mathbf{x}_u^H(w)\right] = \mathbf{R}_c(w) + \sigma_n^2\mathbf{I}_{NM}(w), \tag{15}$$

where the CCM $\mathbf{R}_c(w)$ is

$$\mathbf{R}_c(w) = \mathbf{V}(w)\mathbf{P}(w)\mathbf{V}^H(w) \tag{16}$$

with

$$\mathbf{V}(w) = [\mathbf{v}(\varphi_{c,1}(w), f_{c,1}(w)), \ldots, \mathbf{v}(\varphi_{c,N_c}(w), f_{c,N_c}(w))] \tag{17}$$

and

$$\mathbf{P}(w) = diag([p_1, p_2, \ldots, p_{N_c}]^T), p_i = E(|a_{c,i}|^2). \tag{18}$$

Substituting (13) into (16), $\mathbf{R}_c(w)$ can be updated as

$$\mathbf{R}_c(w) = \begin{bmatrix} R_{0,0}(w) & R_{0,1}(w) & \cdots & R_{0,NM-1}(w) \\ R_{1,0}(w) & R_{1,1}(w) & \cdots & R_{1,NM-1}(w) \\ \vdots & \vdots & \ddots & \vdots \\ R_{NM-1,0}(w) & R_{NM-1,1}(w) & \cdots & R_{NM-1,NM-1}(w) \end{bmatrix}, \tag{19}$$

where

$$\begin{aligned} &R_{(l_1M+r_1-1),(l_2M+r_2-1)}(w) \\ &= \sum_{i=1}^{N_c} p_k \exp(j[k(n_{l_1} - n_{l_2})d\cos(\theta_i) \\ &\quad + k(m_{r_1-1} - m_{r_2-1})T2v\cos(\theta_i)]) \end{aligned} \tag{20}$$

with $l_1, l_2 = 0, \cdots, N-1, r_1, r_2 = 1, \cdots, M$.

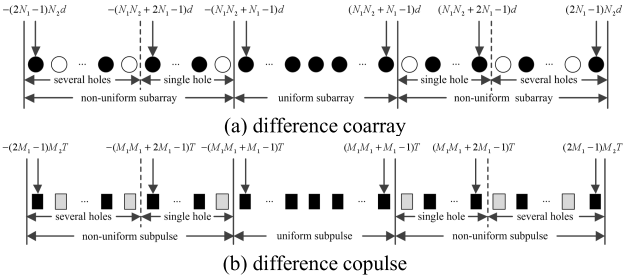

(a) difference coarray

(b) difference copulse

Filled circle stands for physical sensors and empty circle represents empty space. Filled rectangle stands for transmitting pulses and empty rectangle represents empty space.

FIGURE 2. Difference coarray and copulse.

Definition 1 (Difference Coarray): The difference coarray $\mathbb{D}$ of a sparse array $\mathbb{A}$ can be defined as

$$\mathbb{D} = \{d_{n1} - d_{n2} \,|d_{n1}, d_{n2} \in \mathbb{A}\}. \tag{21}$$

Definition 2 (Difference Copulse): For a sparse pulse train $\mathbb{P}$, its difference copulse $\mathbb{Q}$ is

$$\mathbb{Q} = \{q_{m1} - q_{m2} \,|q_{m1}, q_{m2} \in \mathbb{P}\}. \tag{22}$$

Thus, $\hat{n}_{kl} = n_{l_1} - n_{l_2}$ and $\hat{p}_{kl} = p_k - p_l$ in (20) can be regarded as the virtual sensor and pulse positions of the difference coarray and copulse respectively, and their determine the value of $R_{(l_1M+r_1-1),(l_2M+r_2-1)}(w)$. The virtual sensor and pulse positions corresponding to the coprime structure in Fig. 1 can be expressed

$$\mathbb{D}_l = \{-(2N_1-1)N_2, -(2N_1-2)N_2, \cdots, 2N_1-1)N_2\}, \tag{23}$$

$$\mathbb{Q}_l = \{-(2M_1-1)M_2, -(2M_1-2)M_2, \cdots, (2M_1-1)M_2\}. \tag{24}$$

As we can see in the Fig. 2 (a) shows, the uniform part in $\mathbb{D}_l$ is only from $-(N_1N_2 + N_1 - 1)$ to $(N_1N_2 + N_1 - 1)$. And two non-uniform subarrays which can be subdivided into a single hole subarray and several holes subarrays are exactly symmetrical. Difference copulse has the same configuration and property as difference coarray, as Fig. 2 (b) shows. It's remarkable that the traditional algorithms only utilize the uniform parts of the difference structure in the coprime configuration, which can be regarded as a virtual ULA with $\bar{N} = 2N_1N_2 + 2N_1 + 1$ sensors and d spacing and a virtual CPI with $\bar{M} = 2M_1M_2 + 2M_1 + 1$ pulses and T spacing. However, the non-uniform subarrays and subpulses are abandoned, resulting in the loss of DOF, that is, the decline of resolution. If the holes in the difference coarray and copulse can be filled, the number of available virtual sensors and pulses can be significantly increased to obtain greater DOF in the spatial and temporal domain.

B. MUTUAL COUPLING

In practical environment, the electromagnetic coupling among the sensors in radar signal processing is potentially catastrophic. The electromagnetic coupling effect relates to

the inter-sensors spacing. In order to analyze it, we define the weight function $w(m)$ of sparse array $\mathbb{A}$ as the number of sensor pairs which generates the index m:

$$w(m) = \{(d_{n1}, d_{n2}) \in \mathbb{A}^2, d_{n1} - d_{n2} = m\}. \quad (25)$$

Therefore, we can conclude that the first three weight functions $w(m)$ of the coprime array are all 2. Nevertheless, the ULA weight functions $w(m)$ at $m = 1, 2, 3$ are $w(1) = N-1$, $w(2) = N-2$, $w(3) = N-3$, $N \geq 3$. When $N > 5$, the first three weight functions $w(m)$ of coprime array are less than those of ULA, which is illustrated evidently that the coprime array has an advantage over ULA in alleviating mutual coupling effect.

III. THE PROPOSED METHOD

In this section, we reinforce the coprime sampling structure via dual-frequency operation in order to extend uniform virtual coarrays and copulses simultaneously.

A. THE PROPOSED METHOD

Assuming that the frequency range of the signal source is enough to cover two operation frequencies in the coprime sampling structure, i.e. the reference frequency w_0 and the additional operation frequency w_h. Considering the coprime sampling structure as shown in Fig. 1, it is assumed that if $w = w_0$ then $d_0 = \lambda/2$, $k = k_0$ and $T = T_0$. In $w_h = \alpha_h w_0$, thus (1) changes into

$$\mathbf{x}_u(w_h) = \sum_{i=1}^{N_c} a_{c,i}\mathbf{v}(\varphi_{c,i}(w_h)) \otimes \mathbf{v}(f_{c,i}(w_h)) + \mathbf{n}(w_h), \quad (26)$$

where $\mathbf{v}(\varphi_{c,i}(w_h), f_{c,i}(w_h))$ is the clutter space-time steering vector in w_h, whose elements are

$$\begin{aligned} s_{lM+r-1,i}(w_h) &= \exp(2\pi j(n_l\varphi_{c,i}(w_h) + m_{r-1}f_{c,i}(w_h))) \\ &= \exp(j(k_h n_l d_0 \cos(\theta_i) + k_h m_{r-1} T_0 2v \cos(\theta_i))), \end{aligned} \quad (27)$$

where $l = 0, \cdots, N-1$, $r = 1, \cdots, M$, $i = 1, \cdots, N_c$. $k_h = w_h/c$ is the wave number in w_h. Due to $k_h = \alpha_h k_0$, (27) can be rewritten as

$$\begin{aligned} s_{lM+r-1,i}(w_h) = \exp(j(&k_0\alpha_h n_l d_0 \cos(\theta_i) \\ &+ k_0\alpha_h m_{r-1} T_0 2v \cos(\theta_i))). \end{aligned} \quad (28)$$

Comparing (14) with (28), the space-time steering matrix associated with w_h is equivalent to the space-time steering matrix in w_0 after scale transformation. At this point, the positions of *ith* sensor and *jth* pulse are $\alpha_h n_i d_0$ and $\alpha_h m_j T_0$ respectively. Therefore, we can obtain the following equations:

$$\begin{aligned} \mathbb{D}(w_h) = &\{\pm a_h(N_1 p_2 d_0 - N_2 p_1 d_0)\}, \\ &1 \leq p_1 \leq 2N_1 - 1,\ 0 \leq p_2 \leq N_2 - 1, \end{aligned} \quad (29)$$

$$\begin{aligned} \mathbb{Q}(w_h) = &\{\pm\alpha_h(M_1 q_2 T_0 - M_2 q_1 T_0)\}, \\ &1 \leq q_1 \leq 2M_1 - 1,\ 0 \leq q_2 \leq M_2 - 1. \end{aligned} \quad (30)$$

When $w_h > w_0$ ($\alpha_h > 1$), the difference coarray and copulse will spread, otherwise they will shrink. Therefore, a reasonable additional frequency can produce expected virtual sensors and pulses in the holes positions of the difference structure. For two holes with locations $\pm(N_1N_2 + N_1)$ as shown in Fig. 2 (a), the additional operation frequency can be selected as

$$w_h = \frac{N_1N_2 + N_1}{N_1N_2 + N_1 + 1} w_0. \quad (31)$$

This means that two subarrays adjacent to the holes lateral shrink to the locations of hole, thus filling the holes. In fact, the two holes with $\pm(N_1N_2 + N_1)$ can be filled by any virtual sensors. Considering the effect of additional operation frequency on system complexity and fluctuations signal source characteristics, the additional frequency is required to be close to and less than the reference frequency w_0. Therefore, the additional frequency in (31) is the optimal for filling the two holes with $\pm(N_1N_2 + N_1)$. At this time, the difference virtual uniform subarray can obtain $2N_1N_2 + 4N_1 - 1$ DOF, which improve the array DOF by $2N_1$ comparing with the signal-frequency operation. By using the similar process, two holes with $\pm(M_1M_2 + M_1)$ in the difference copulse shown in Fig. 2 (b) can also be filled, and the optimal additional operation frequency also is

$$w_{h2} = \frac{M_1M_2 + M_1}{M_1M_2 + M_1 + 1} w_0. \quad (32)$$

When the array and pulse have the same structure configuration, the structures of their difference coarray and copulse are similar. We can use only one additional frequency to fill the holes in the difference coarray and copulse at the same time. In particular, the elements of the CCM corresponding to the difference coarray from $-(N_1N_2 + N_1 - 1)$ to $(N_1N_2 + N_1 - 1)$ and the difference copulse train from $-(M_1M_2 + M_1 - 1)$ to $(M_1M_2 + M_1 - 1)$ in w_0 are

$$R(w_0) = \sum_{i=1}^{N_c} p_k \exp(j[k_0\hat{n}_{kl} d \cos(\theta_i) + k_0\hat{p}_{kl} T 2v \cos(\theta_i)]), \quad (33)$$

where

$$\hat{n}_{kl} = -(N_1N_2 + N_1 - 1), \cdots, (N_1N_2 + N_1 - 1), \quad (34)$$

$$\hat{p}_{kl} = -(M_1M_2 + M_1 - 1), \cdots, (M_1M_2 + M_1 - 1). \quad (35)$$

Thus, the elements of the CCM with the additional frequency w_h are

$$R(w_h) = \sum_{i=1}^{N_c} p_k \exp(j[k_h\hat{n}_{kl} d \cos(\theta_i) + k_h\hat{p}_{kl} T 2v \cos(\theta_i)]). \quad (36)$$

According to $k_0/k_h = w_0/w_h$, we can show that,

$$\begin{aligned} R(w_h) = \sum_{i=1}^{N_c} p_k \exp(j[&\frac{k_0}{w_0} w_h \hat{n}_{kl} d \cos(\theta_i) \\ &+ \frac{k_0}{w_0} w_h \hat{p}_{kl} T 2v \cos(\theta_i)]), \end{aligned} \quad (37)$$

and further we have,

$$R(w_h) = \sum_{i=1}^{N_c} p_k \exp(j[k_0 \frac{N_1N_2+N_1}{N_1N_2+N_1+1}\hat{n}_{kl} d\cos(\theta_i) + k_0 \frac{M_1M_2+M_1}{M_1M_2+M_1+1}\hat{p}_{kl} T 2v\cos(\theta_i)]). \quad (38)$$

When $\hat{n}_{kl} = N_1N_2+N_1+1, \hat{p}_{kl} = M_1M_2+M_1+1, N_1 = M_1$, and $N_2 = M_2$, the above equation (38) can be rewritten as

$$R(w_h) = \sum_{i=1}^{N_c} p_k \exp(j[k_0(N_1N_2+N_1)d\cos(\theta_i) + k_0(M_1M_2+M_1)T2v\cos(\theta_i)]) \quad (39)$$

that is the data of CCM corresponding to the virtual difference $\hat{n}_{kl} = N_1N_2+N_1$ coarray and $\hat{p}_{kl} = M_1M_2+M_1$ copulse in w_0.

To avoid the complex calculation of spatial-temporal smoothing operation, the virtual CCM is obtained by means of the matrix increment-rank approach, i.e.,

$$\mathbf{R}_c(w_0) = \begin{bmatrix} R_{0,0}(w_0) & R_{0,1}(w_0) & \cdots & R_{0,D-1}(w_0) \\ R_{1,0}(w_0) & R_{1,1}(w_0) & \cdots & R_{1,D-1}(w_0) \\ \vdots & \vdots & \ddots & \vdots \\ R_{D-1,0}(w_0) & R_{D-1,1}(w_0) & \cdots & R_{D-1,D-1}(w_0) \end{bmatrix}, \quad (40)$$

where $\hat{N} = 2N_1N_2+4N_1-1$, $\hat{M} = 2M_1M_2+4M_1-1$, and $D = \hat{N}\hat{M}$. $\mathbf{R}_c$ can be thought of as the virtual CCM estimation corresponding to $\hat{N}$ sensors with inter-sensors spacing d_0 and $\hat{M}$ pulses with fixed PRI T_0 during a CPI. Compared with the single-frequency mode, the dual-frequency mode can improve the system DOF by D_I. In this way, multiple holes in the non-uniform several holes subarrays and subpulses can be filled by using multiple additional operation frequencies, but the DOFs elevated by these additional frequencies are less than D_I. Therefore, this paper focuses on the design of dual-frequency operation mode for single hole parts.

According to the minimum variance distortion less response (MVDR) criterion, the optimal STAP weight vectors can be computed as

$$\mathbf{w} = \frac{\mathbf{R}_u^{-1}(w_0)\mathbf{v}_t}{\mathbf{v}_t^H \mathbf{R}_u^{-1}(w_0)\mathbf{v}_t}, \quad (41)$$

where

$$\mathbf{R}_u(w_0) = \mathbf{R}_c(w_0) + \sigma_n^2 \mathbf{I}_{DD}(w_0) \quad (42)$$

and $\mathbf{v}_t$ represents the space-time steering vector of target.

B. COMPLEXITY ANALYSIS

In this section, the computational complexities of the traditional STAP (T-STAP) [1], the traditional coprime STAP (C-STAP) [25], and the proposed algorithm (DFC-STAP), are analyzed. Their main complexities originate from the filter weights computation, which are $O((NM)^3)$, $O((\bar{N}\bar{M})^3)$, $O((\hat{N}\hat{M})^3)$ respectively. Since the DFC-STAP estimates the CCM by the dual-frequency mode, the computational burden of this part is more than twice that of the C-STAP. Therefore, the complexity of the DFC-STAP is larger than that of the C-STAP. However, the performance of the DFC-STAP is much better than the C-STAP.

IV. SIMULATION RESULTS

In this section, we select three STAP methods: the T-STAP, the C-STAP and the DFC-STAP, and then compare their performances. There are $N = 6$ physical sensors and $M = 6$ pulses in the radar system, where $\lambda = 0.05$m, $T_0 = 0.25$ms, $N_c = 361$, $v = 50m/s$, $\sigma_n^2 = 1$ and $w = w_0$. We set $N_1 = M_1 = 2$ and $N_2 = M_2 = 3$ for the C-STAP. The normalized angle and Doppler frequency of target are 0.1 and -0.2 respectively. The clutter to noise ratio is 30dB, and the signal to noise ratio is set to 0dB. All simulation results are averages over 100 Monte Carlo experiments.

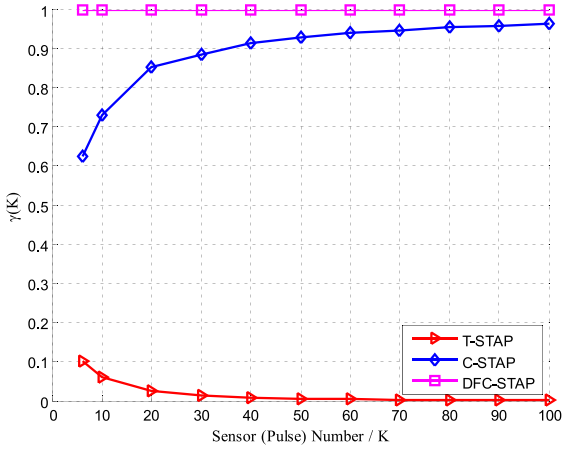

FIGURE 3. The DOF ratio with the sensor/pulse number K varying from 6 to 100.

A. DOF

To visually compare the ability of various algorithms to obtain DOF, we define the DOF ratio as

$$\gamma(K) = L(K)/L_{DFC}(K), \quad (43)$$

where $L_{DFC}(K)$ denotes the maximum DOF of the proposed algorithm when the total number of physical sensors and pulses are both K, i.e. $M = N = K$. The DOF capacity varies proportional with $\gamma(K)$ to some extent. From Fig. 3 which illustrates the $\gamma(K)$ with K varying from 6 to 100, the C-STAP and DFC-STAP have higher DOF than the T-STAP. However, the DOF of the C-STAP is significantly lower than that of the DFC-STAP. Compared with other two methods, the DFC-STAP is of the advantages of high DOF in the small K.

B. BEAMPATTERNS

In this experiment, we depict the beampatterns with different methods. Fig 4. and Fig 5. give the space-time beampatterns with and without the mutual coupling, respectively.

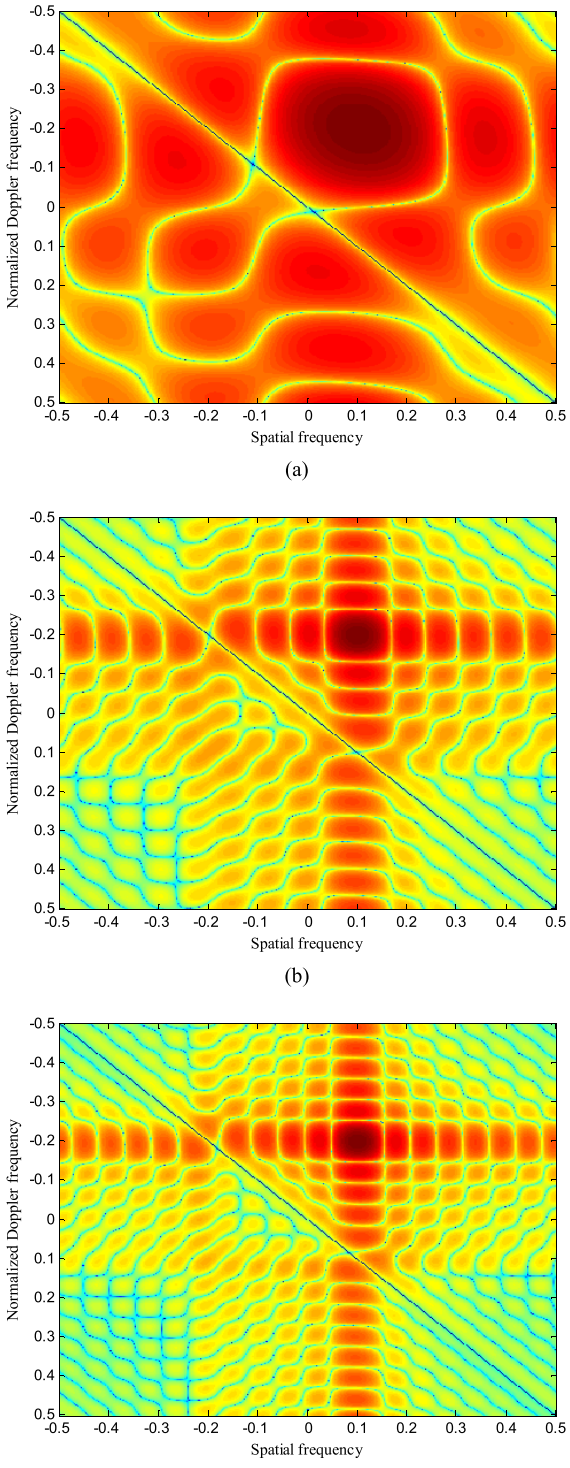

FIGURE 4. Space-time Beampatterns without the mutual coupling (a) T-STAP (b) C-STAP (c) DFC-STAP.

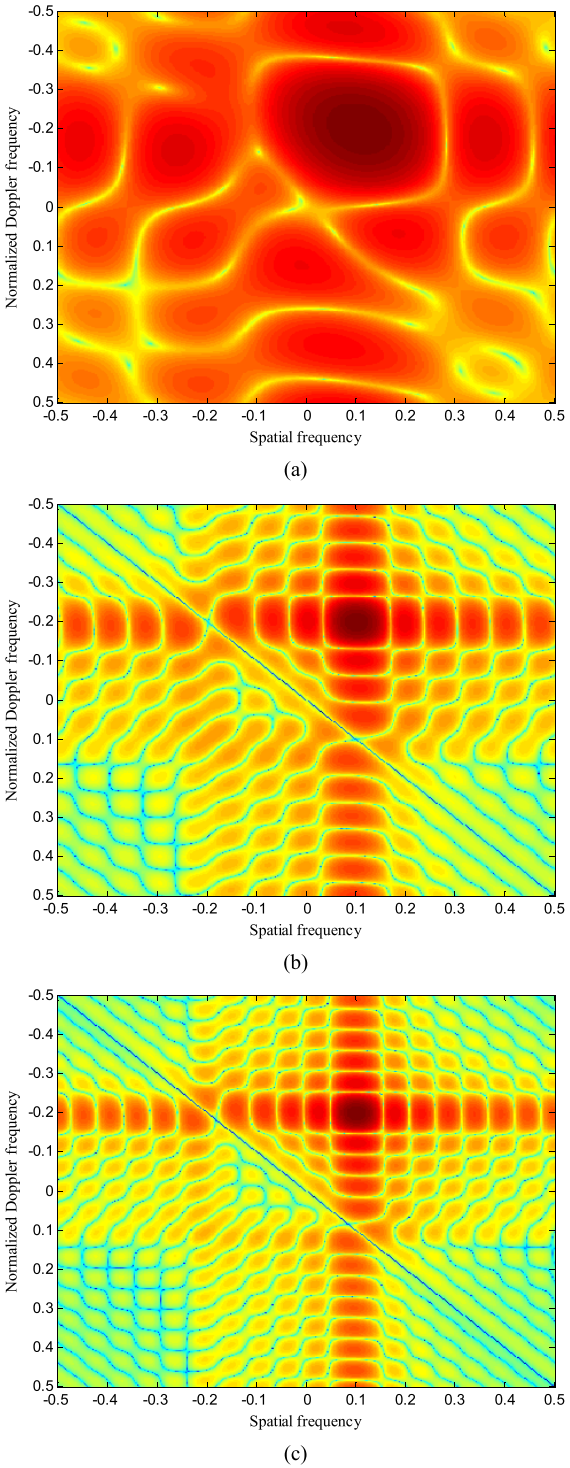

FIGURE 5. Space time Beampatterns with the mutual coupling (a) T-STAP (b) C-STAP (c) DFC-STAP.

The MC-T-STAP, MC-C-STAP and MC-DFC-STAP are the abbreviation of the algorithms corresponding to the T-STAP, C-STAP and DFC-STAP in the presence of the mutual coupling. We set $\mathbf{c} = [1, 0.5e^{j\pi/4}, 0.25e^{j0.7\pi}, 0.5e^{j0.7\pi}/3]^T$ and $B = 3$. Due to the mutual coupling effect, the T-STAP can not suppress the clutter in main clutter area, and its performance is seriously deteriorated. Although the C-STAP can suppress the main clutter and detect the signal, whose temporal and spatial resolutions are lower than that of the FDC-STAP in Fig. 6. The FDC-STAP can form the optimal space-time beampattern at the target location and a deep notch at the main

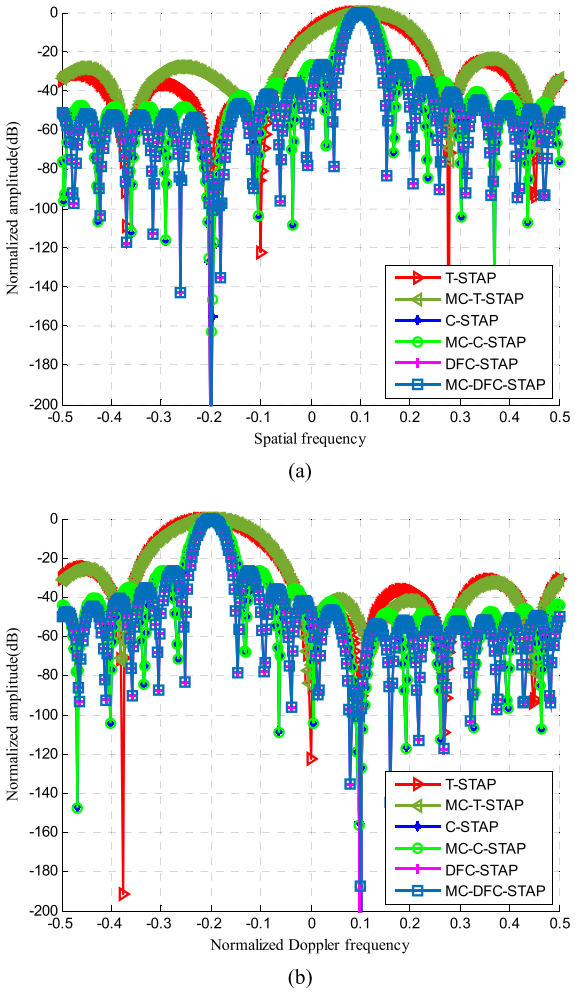

FIGURE 6. Beampatterns (a) Spatial domain (b) Doppler domain.

clutter area, whether or not there is mutual coupling. This is because there are virtual sensors and pulses missing at ± 8 position in difference coarray and copulse for the C-STAP. Therefore, the optimal filter weight vector can be seen as a result from a virtual ULA with 15 sensors and pulse trains with 15 pulses in a CPI, and have 255 DOF at the working frequency of w_0. According to (31), the FDC-STAP chooses $w_h = 8/9w_0$ to fill the holes at ± 8 position. We can gain a virtual ULA with 19 sensors and pulses trains with 19 pulses, thus the DOF of the filter is increased to 361. The DOF of FDC-STAP increases 136 compared with the C-STAP by an additional operation frequency.

C. SINR

Finally, Fig.7 shows the output SINR performance against the normalized Doppler frequency with or without mutual coupling. The FDC-STAP uses dual-frequency operation mode to fill the holes of the difference structure and improve the filter DOF, and its output SINR performance is optimal, C-STAP, T-STAP in turn. Due to the inter-sensors of coprime array is larger than that of ULA, and its mutual coupling effect

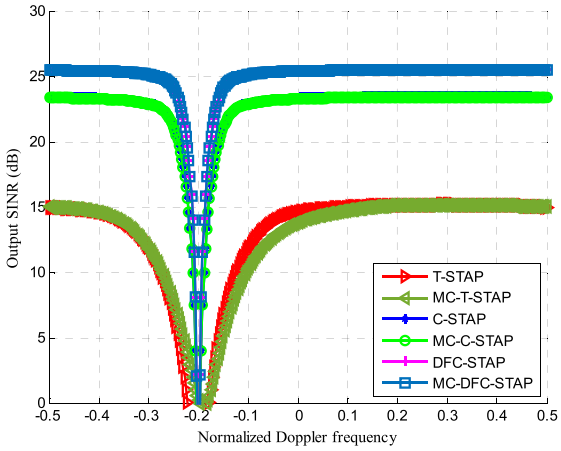

FIGURE 7. Output SINR.

is weaker, the output SINR performance of C-STAP and FDC-STAP is almost unaffected under the condition of the mutual coupling. However, the output SINR performance of T-STAP deteriorates seriously in the mutual coupling.

V. CONCLUSION

In this paper, a STAP algorithm with the dual-frequency coprime structure is proposed, which can obtain more uniform virtual sensors and pulses than by the single-frequency operation to improve the DOF and reduce the mutual coupling effect. Under N physical sensors and M physical pulses conditions, the dual-frequency operation can improve the system DOF by D_I. Due to the single additional operation frequency, the proposed dual-frequency operation extends the system operational bandwidth and introduces the fluctuations signal source characteristics to increase the complexity and cost of the system as well as the filter optimal weight vector estimation error. In this paper, we choose the additional operation frequency which is lower than and close to the reference frequency, which can minimize the adverse effects of dual-frequency operation as much as possible. In the following work, we will focus on the influence of the fluctuations signal source characteristics on the filter weight vector estimation, and study the corresponding processing methods.

REFERENCES

[1] W. L. Melvin, "A STAP overview," *IEEE Aerosp. Electron. Syst. Mag.*, vol. 19, no. 1, pp. 19–35, Jan. 2004.
[2] Y. Feng, T. Shan, S. Liu, and R. Tao, "Interference suppression using joint spatio-temporal domain filtering in passive radar," in *Proc. IEEE Radar Conf. (RadarCon)*, Arlington, VA, USA, May 2015, pp. 1156–1160.
[3] M. Liu, L. Zou, X. Yu, Y. Zhou, X. Wang, and B. Tang, "Knowledge aided covariance matrix estimation via Gaussian kernel function for airborne SR-STAP," *IEEE Access*, vol. 8, pp. 5970–5978, 2020.
[4] J. R. Guerci, J. S. Goldstein, and I. S. Reed, "Optimal and adaptive reduced-rank STAP," *IEEE Trans. Aerosp. Electron. Syst.*, vol. 36, no. 2, pp. 647–663, Apr. 2000.
[5] B. D. Carlson, "Covariance matrix estimation errors and diagonal loading in adaptive arrays," *IEEE Trans. Aerosp. Electron. Syst.*, vol. 24, no. 4, pp. 397–401, Jul. 1988.

[6] C. H. Gierull and B. Balaji, "Minimal sample support space-time adaptive processing with fast subspace techniques," *IEE Proc.-Radar, Sonar Navigat.*, vol. 149, no. 5, pp. 209–220, Oct. 2002.
[7] A. M. Haimovich and Y. Bar-Ness, "An eigenanalysis interference canceler," *IEEE Trans. Signal Process.*, vol. 39, no. 1, pp. 76–84, Jan. 1991.
[8] I. S. Reed, J. D. Mallett, and L. E. Brennan, "Rapid convergence rate in adaptive arrays," *IEEE Trans. Aerosp. Electron. Syst.*, vol. AES-10, no. 6, pp. 853–863, Nov. 1974.
[9] Y.-L. Wang, Y.-N. Peng, and Z. Bao, "Space-time adaptive processing for airborne radar with various array orientations," *IEE Proc.-Radar, Sonar Navigat.*, vol. 144, no. 6, pp. 330–340, Dec. 1997.
[10] X. Wang, Z. Yang, J. Huang, and R. C. de Lamare, "Robust two-stage reduced-dimension sparsity-aware STAP for airborne radar with coprime arrays," *IEEE Trans. Signal Process.*, vol. 68, pp. 81–96, Dec. 2020.
[11] R. D. Brown, R. A. Schneible, M. C. Wicks, H. Wang, and Y. Zhang, "STAP for clutter suppression with sum and difference beams," *IEEE Trans. Aerosp. Electron. Syst.*, vol. 36, no. 2, pp. 634–646, Apr. 2000.
[12] J. R. Roman, M. Rangaswamy, D. W. Davis, Q. Zhang, B. Himed, and J. H. Michels, "Parametric adaptive matched filter for airborne radar applications," *IEEE Trans. Aerosp. Electron. Syst.*, vol. 36, no. 2, pp. 677–692, Apr. 2000.
[13] K. J. Sohn, H. Li, and B. Himed, "Parametric Rao test for multichannel adaptive signal detection," *IEEE Trans. Aerosp. Electron. Syst.*, vol. 43, no. 3, pp. 920–933, Jul. 2007.
[14] P. Wang, H. Li, and B. Himed, "Parametric rao tests for multichannel adaptive detection in partially homogeneous environment," *IEEE Trans. Aerosp. Electron. Syst.*, vol. 47, no. 3, pp. 1850–1862, Jul. 2011.
[15] C. Jiang, H. Li, and M. Rangaswamy, "Conjugate gradient parametric detection of multichannel signals," *IEEE Trans. Aerosp. Electron. Syst.*, vol. 48, no. 2, pp. 1521–1536, Apr. 2012.
[16] P. Parker and A. Swindlehurst, "Space-time autoregressive filtering for matched subspace STAP," *IEEE Trans. Aerosp. Electron. Syst.*, vol. 39, no. 2, pp. 510–520, Apr. 2003.
[17] P. Wang, H. Li, and B. Himed, "A Bayesian parametric test for multichannel adaptive signal detection in nonhomogeneous environments," *IEEE Signal Process. Lett.*, vol. 17, no. 4, pp. 351–354, Apr. 2010.
[18] P. Wang, H. Li, and B. Himed, "Knowledge-aided parametric tests for multichannel adaptive signal detection," *IEEE Trans. Signal Process.*, vol. 59, no. 12, pp. 5970–5982, Dec. 2011.
[19] P. Wang, Z. Sahinoglu, M.-O. Pun, and H. Li, "Persymmetric parametric adaptive matched filter for multichannel adaptive signal detection," *IEEE Trans. Signal Process.*, vol. 60, no. 6, pp. 3322–3328, Jun. 2012.
[20] Q. T. Zhang, "Asymptotic performance analysis of information-theoretic criteria for determining the number of signals in spatially correlated noise," *IEEE Trans. Signal Process.*, vol. 42, no. 6, pp. 1537–1539, Jun. 1994.
[21] A. P. Liavas and P. A. Regalia, "On the behavior of information theoretic criteria for model order selection," *IEEE Trans. Signal Process.*, vol. 49, no. 8, pp. 1689–1695, Aug. 2001.
[22] B. Nadler, "Nonparametric detection of signals by information theoretic criteria: Performance analysis and an improved estimator," *IEEE Trans. Signal Process.*, vol. 58, no. 5, pp. 2746–2756, May 2010.
[23] E. Fishler and H. Messer, "On the use of order statistics for improved detection of signals by the MDL criterion," *IEEE Trans. Signal Process.*, vol. 48, no. 8, pp. 2242–2247, Aug. 2000.
[24] Q. Ding and S. Kay, "Inconsistency of the MDL: On the performance of model order selection criteria with increasing signal-to-noise ratio," *IEEE Trans. Signal Process.*, vol. 59, no. 5, pp. 1959–1969, May 2011.
[25] D. F. Schmidt and E. Makalic, "The consistency of MDL for linear regression models with increasing Signal-to-Noise ratio," *IEEE Trans. Signal Process.*, vol. 60, no. 3, pp. 1508–1510, Mar. 2012.
[26] B. Friedlander and A. J. Weiss, "Direction finding in the presence of mutual coupling," *IEEE Trans. Antennas Propag.*, vol. 39, no. 3, pp. 273–284, Mar. 1991.
[27] C.-M.-S. See and B.-K. Poh, "Parametric sensor array calibration using measured steering vectors of uncertain locations," *IEEE Trans. Signal Process.*, vol. 47, no. 4, pp. 1133–1137, Apr. 1999.
[28] F. Sellone and A. Serra, "A novel online mutual coupling compensation algorithm for uniform and linear arrays," *IEEE Trans. Signal Process.*, vol. 55, no. 2, pp. 560–573, Feb. 2007.
[29] M. Liu, X. Wang, and L. Zou, "Robust STAP with reduced mutual coupling and enhanced DOF based on super nested sampling structure," *IEEE Access*, vol. 7, pp. 175420–175428, 2019.
[30] Z. T. Huang, Z. M. Liu, J. Liu, and Y. Y. Zhou, "Performance analysis of MUSIC for non-circular signals in the presence of mutual coupling," *IET Radar, Sonar Navigat.*, vol. 4, no. 5, pp. 703–711, 2010.
[31] S. Liu, Y. Ma, and T. Shan, "Segmented discrete polynomial-phase transform with coprime sampling," in *Proc. IET Radar Conf. (IRC)*, Nanjing, China, 2018, pp. 5619–5621.
[32] Z. Tan, Y. C. Eldar, and A. Nehorai, "Direction of arrival estimation using co-prime arrays: A super resolution viewpoint," *IEEE Trans. Signal Process.*, vol. 62, no. 21, pp. 5565–5576, Nov. 2014.
[33] S. Qin, Y. D. Zhang, and M. G. Amin, "Generalized coprime array configurations for Direction-of-Arrival estimation," *IEEE Trans. Signal Process.*, vol. 63, no. 6, pp. 1377–1390, Mar. 2015.
[34] C. L. Liu and P. P. Vaidyanathan, "Remarks on the spatial smoothing step in coarray MUSIC," *IEEE Trans. Signal Process.*, vol. 63, no. 6, pp. 1377–1390, Mar. 2015.

MINGXIN LIU was born in Ningxia, China. He received the B.S. degree from Northeast Electric Power University, Jilin, China, in 2009, and the M.S. degree from the University of Electronic Science and Technology of China (UESTC), Chengdu, China, in 2012, where he is currently pursuing the Ph.D. degree. He is also a Lecturer with the School of General Aviation, Chengdu Aeronautic Polytechnic. His research interests include array signal processing, adaptive signal processing, and radar signal processing.

BIN TANG (Member, IEEE) was born in Sichuan, China. He received the B.S. degree in electronic engineering from Nanchang Hangkong University, in 1997, and the M.S. degree in automation engineering and the Ph.D. degree in electronic engineering from the University of Electronic Science and Technology of China (UESTC), in 2003 and 2016, respectively. From 2015 to 2016, he was a Visiting Scholar with the University of California, San Diego. He is currently an Associate Professor with the School of General Aviation, Chengdu Aeronautic Polytechnic, Chengdu, China. His current research interests include array signal processing, adaptive signal processing, signal detection, and embedded systems and applications.

XIAOXIA ZHENG was born in Sichuan, China. She received the B.S. degree in computer engineering from North China Electric Power University, in 1999, and the M.S. degree in computer engineering from UESTC, in 2002. From 2000 to 2002, she was a Communication Software Engineer with Huawei. From 2002 to 2005, she worked as an Embedded System Engineer with ZTE. From 2005 to 2015, she worked as an Embedded System Engineer with Motorola. She is currently an Assistant Professor with the School of General Aviation, Chengdu Aeronautic Polytechnic. Her current research interests include embedded system software design, computer communication, and software test.

QIANG WANG was born in Wuhan, China. He received the B.S. degree from Nanchang Hangkong University, Nanchang, China, in 2013, and the M.S. degrees from the University of Electronic Science and Technology of China (UESTC), Chengdu, China, in 2017. He is currently a Lecturer with the School of General Aviation, Chengdu Aeronautic Polytechnic. His research interests include multi-sensor fusion, adaptive signal processing, and reliable navigation and control.

SIYUAN WANG was born in Chengdu, China. He received the B.S. and M.S. degrees from Chongqing University, Chongqing, China, in 2012 and 2015, respectively. He is currently a Lecturer with the School of General Aviation, Chengdu Aeronautic Polytechnic. His research interests include mechatronics and aircraft hydraulic technology.

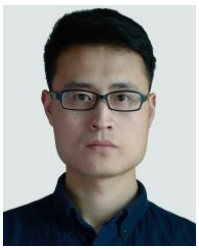

XU WANG was born in Sichuan, China. He received the B.S. degree from Shenyang Aerospace University, Liaoning, China, in 2013, and the M.S. degree from Air Force Engineering University, Xi'an, China, in 2016. He is currently a Lecturer with the School of General Aviation, Chengdu Aeronautic Polytechnic. His research interests include aircraft design, flight mechanics, and flight dynamics.

MENGXU FANG was born in Henan, China. He received the B.S. degree from Zhengzhou University, Henan, China, in 2009, and the M.S. degree from of the Nanchang Hangkong University (UCHU) of China, Nanchang, China, in 2012. He is currently a Lecturer with the School of Information Engineering, Chengdu Aeronautic Polytechnic. His research interests include wireless communication technology and signal processing.

JING ZHU was born in Shanxi, China. He received the B.S. degree in microelectronics manufacturing engineering and the M.S. degree in mechatronic engineering from the Guilin University of Electronic Technology, Guilin, China, in 2010 and 2013, respectively. He is currently a Lecturer with the School of Information Engineering, Chengdu Aeronautic Polytechnic. His research interests include optimization, machine learning, and machine vision.

CHENGLONG FENG was born in Sichuan, China. He received the degree from the PLA Air Force No.1 Aviation University, Xinyang, China, in 2013. He is currently a Lecturer with the School of General Aviation, Chengdu Aeronautic Polytechnic. His research interests include array signal processing, and typical helicopter fault diagnosis and removal.